5.3 SPECTRAL BIDIRECTIONAL REFLECTANCE OF ANTARCTIC SNOW: MEASUREMENTS AND PARAMETERIZATION

Stephen R. Hudson*, Stephen G. Warren, Richard E. Brandt, and Thomas C. Grenfell
University of Washington, Seattle, Washington
Delphine Six
Laboratoire de Glaciologie et Géophysique de l'Environnement, Saint Martin d'Hères, France

1. INTRODUCTION

The bidirectional reflectance distribution function (BRDF) of snow was measured from a 32-meter tower at Dome C, at latitude 75°S on the East Antarctic Plateau. These measurements were made at 96 solar zenith angles between 51° and 87°, and cover wavelengths 350—2400 nm, with 3- to 30-nanometer resolution, over the full range of viewing geometry.

From these measurements, parameterizations were developed that allow users to quickly and accurately calculate the anisotropic reflectance function of the East-Antarctic snow surface. The parameterizations cover nearly all viewing angles and are applicable to the high parts of the Antarctic Plateau that have small surface roughness, and, at viewing zenith angles less than 55°, elsewhere on the plateau, where larger surface roughness affects the BRDF at larger viewing angles. The root-mean-squared error of the parameterized reflectances is between 2% and 4% at wavelengths less than 1400 nm and between 5% and 8% at longer wavelengths.

The effect of the snow-surface roughness on the BRDF is examined by comparing the parameterization results with the BRDF predicted by a plane-parallel radiative transfer model for a perfectly flat snow surface. The presence of the roughness reduces the anisotropy of the reflected radiance field. Finally, the effect of having a cloud above the surface is investigated using observations from Dome C of the reflected radiance field from a thin fog layer above the snow surface. It appears that the presence of a cloud or fog layer above the snow surface acts to mask the roughness of the snow, thereby enhancing the anisotropy of the reflected radiance. The full paper is in press (Hudson *et al.*, 2006).

* *Corresponding author address:* Stephen R. Hudson, Box 351640, Dept. of Atmospheric Sciences, University of Washington, Seattle, WA 98195-1640
e-mail: hudson@atmos.washington.edu

2. MEASUREMENTS

The measurements were made at Dome C (75°06′S, 123°18′E, 3200 m MSL) during the summers of 2003/04 and 2004/05. This site is located 15° from the pole, which allowed for measurements at a wide range of solar zenith angles each day, and near a local maximum in elevation, which results in lighter and less directionally-constant winds that produce smaller and less aligned surface roughness features than are found on areas of the Antarctic Plateau with larger surface slopes.

All observations were made from the top of a 32-meter tower to ensure the measurement footprint was large enough to include a representative sample of the rough snow surface. The instrument's field of view has a diameter of 15°, and measurements were centered on viewing zenith angles of 22.5°, 37.5°, 52.5°, 67.5°, and 82.5°. The areas of the footprints at the first four angles were about 70, 110, 260, and 1170 m^2; the footprint at 82.5° extends to the horizon. Even the smallest of these footprints should contain multiple sastrugi.

The radiance measurements were made with an ASD FieldSpec Pro JR spectroradiometer that reports the radiance every 1 nm from 350—2500 nm with a resolution that varies between 3 and 30 nm. The fiber-optic input cable to the ASD was mounted on a goniometer that was manually positioned to measure the radiance coming from 85 different locations on the snow surface during each observation sequence.

Each observation provided radiance measurements over a 255° range of azimuths. The radiance patterns from the entire hemisphere were completed either by reflecting the measurements across the principal plane or by stitching together two patterns with the same solar zenith angle but different solar azimuth angles (one made in the morning and one in the evening on the same or adjacent

days). The reflected radiances were then normalized by the upwelling flux, determined from integrating the reflected radiances (I_r) over the hemisphere, to give the anisotropic reflectance factor (R):

$$R(\theta_\circ,\theta_\mathrm{v},\phi)=\frac{\pi I_r(\theta_\circ,\theta_\mathrm{v},\phi)}{\int_0^{2\pi}\int_0^{\pi/2} I_r(\theta_\circ,\theta_\mathrm{v},\phi)\cos\theta_\mathrm{v}\sin\theta_\mathrm{v}\,\mathrm{d}\theta_\mathrm{v}\,\mathrm{d}\phi},$$

where $\theta_\circ$ is the solar zenith angle, θ_v is the viewing zenith angle, and ϕ is the relative azimuth angle. An isotropic reflector has R = 1 at all angles, regardless of its albedo. Under direct-beam illumination, R is related to the BRDF (ρ) by the albedo (α):

$$R(\theta_\circ,\theta_\mathrm{v},\phi)=\frac{\pi\rho(\theta_\circ,\theta_\mathrm{v},\phi)}{\alpha(\theta_\circ)}.$$

The use of R eliminates the need for either an absolute radiance calibration or an accurate measurement of the downwelling flux.

Examples of the anisotropic reflectance patterns are shown in Figures 1 and 2. Both figures show the patterns at 600 nm, where the albedo is nearly 1, and at 1800 nm, where the albedo is about 0.3; the patterns in Figure 1 were measured under a small solar zenith angle, while those in Figure 2 were measured under a large solar zenith angle. Together these figures illustrate some of the main features of the data. The reflected radiance is greatest when observed near the horizon in the direction of the solar azimuth, and least when observed in the backscatter directions. This anisotropy increases with increasing solar zenith angle and decreases with increasing albedo. At shorter wavelengths in the visible and near-UV, where the amount of diffuse light incident on the snow surface increases, the observed patterns become more isotropic despite the nearly constant albedo in this region of the spectrum.

3. PARAMETERIZATION

Observations of R at 96 different solar zenith angles were used to develop parameterizations that easily calculate the expected value of R on the high Antarctic Plateau. To improve the performance of the parameterizations, the data were divided into six groups based on wavelength, solar zenith angle, and viewing zenith angle, and each group was parameterized separately.

The empirical orthogonal functions (EOFs) of each data subset were used as the basis functions for the parameterization for that subset. Because the EOFs are highly effective at representing a large fraction of the variance in a dataset with a small number of functions, the parameterizations are able to accurately recreate the patterns of R with linear combinations of just the first one to three EOFs, depending on the subset. The EOFs are functions of viewing zenith angle and relative

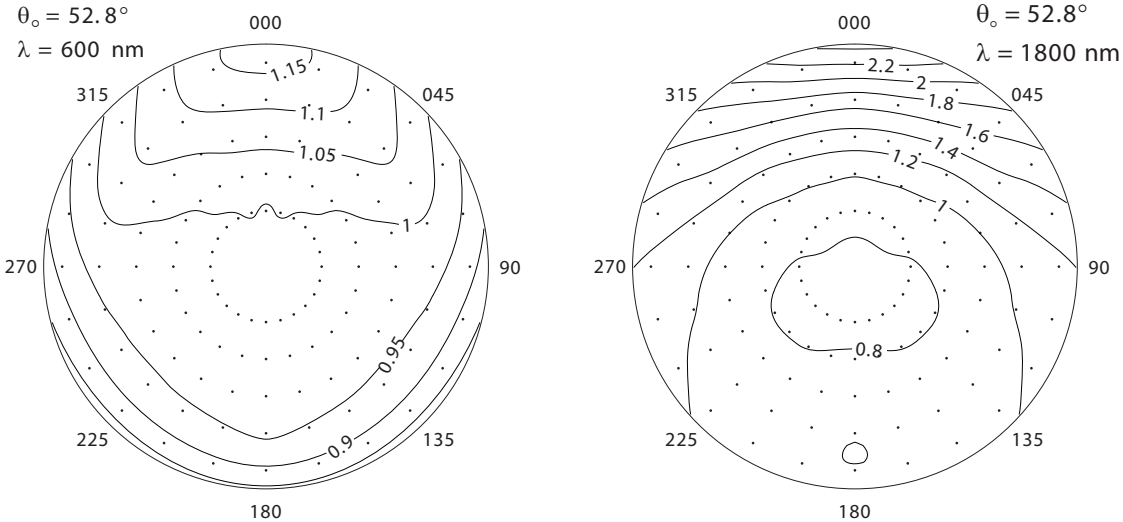

Figure 1. Polar contour plots of the anisotropic reflectance factor (R) at 600 and 1800 nm measured under a solar zenith angle of 52.8°. Dots are placed every 15° in both viewing zenith angle, starting at 22.5°, and relative azimuth angle, starting at 0°, which represents light coming from the azimuth containing the sun.

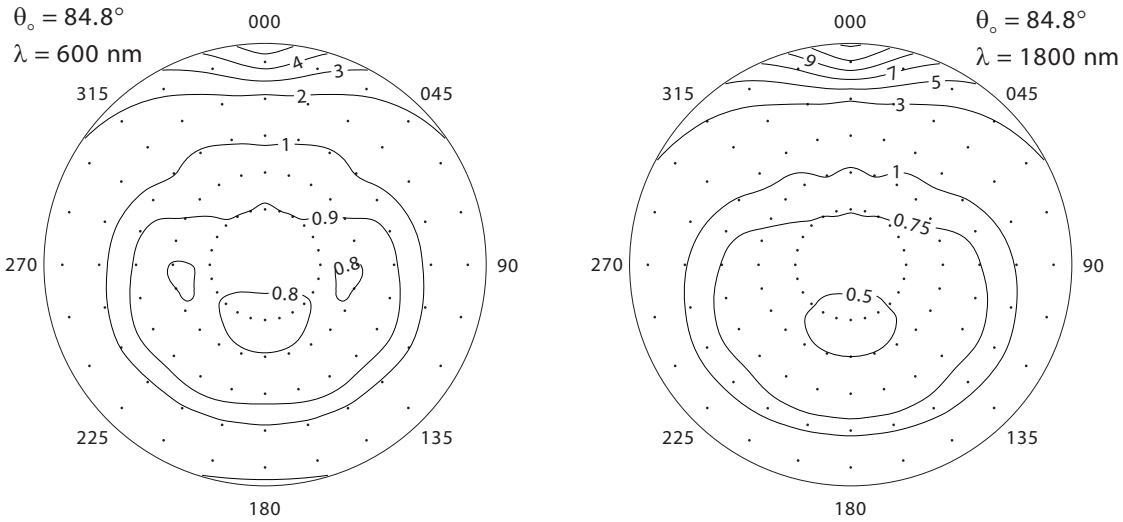

Figure 2. Polar contour plots of the *R* at 600 and 1800 nm measured under a solar zenith angle of 84.8°. The contour interval is smaller for $R < 1$ than for $R > 1$.

azimuth angle. The coefficients that multiply each EOF in the linear combinations are parameterized as functions of solar zenith angle and either wavelength or albedo.

At short wavelengths (350—950 nm), where albedo does not vary much, but the amount of diffuse incident flux due to Rayleigh scattering varies a lot, wavelength proved to be the best predictor of *R*. At longer wavelengths, where albedo varies significantly and there is essentially no Rayleigh scattering, albedo was a much better predictor of *R*. Figure 3 illustrates the tight relationship between *R* and albedo. This figure shows, for three observations on three different days with different solar zenith angles, a very good power-law relationship between the value of *R* observed at the forward reflectance peak as a function of albedo. This relationship holds for albedos between about 0.15 and 0.95. The observations at very low albedos are probably affected by a small signal-to-noise ratio due to the small amount of reflected radiance, and they are not included in the parameterizations. The very high albedos occur in the visible and near-UV, where the large amount of diffuse flux incident on the snow due to Rayleigh scattering reduces the anisotropy of the observed patterns of *R*.

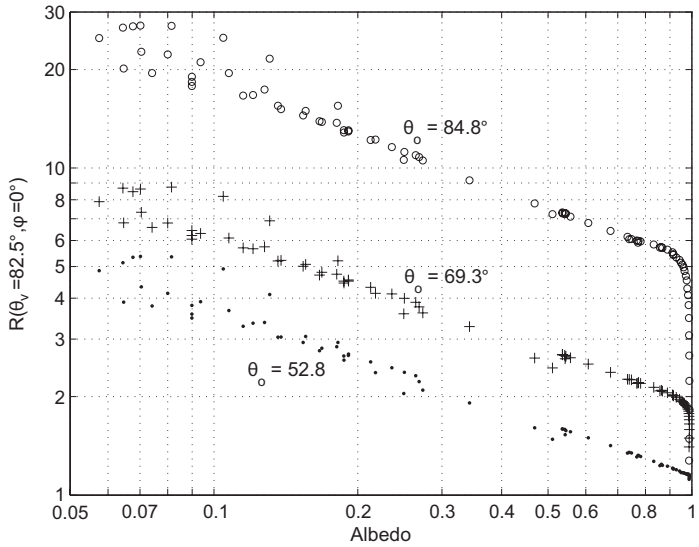

Figure 3. Values of *R* measured at the forward peak, as a function of albedo, for three different solar zenith angles.

Together, the six parameterizations cover all viewing angles at wavelengths 350—1400 nm under solar zenith angles of 51.6° to 86.6°, and at wavelength 1450—2400 nm with albedos greater than 0.15 under solar zenith angles of 51.6° to 75°. The spectral region 1400—1450 nm was excluded because albedo changes extremely rapidly with wavelength there. The root mean squared error of the parameterizations, relative to the observations, ranges from about 2% to 4% for the parameterizations covering wavelengths less than 1400 nm, and from about 6% to 8% for the parameterizations covering longer wavelengths.

4. EFFECT OF SURFACE ROUGHNESS

The observations at Dome C were intentionally made from far enough above the surface to show the BRDF of the naturally rough surface so that they would provide the information necessary for radiative transfer modeling or the use of remote sensing data over the Antarctic Plateau. Warren *et al.* (1998) and Leroux *et al.* (1998) showed some of the effects of surface roughness on the BRDF of snow. Here we examine these effects by comparing the observed reflectance from the natural, rough snow surface with the modeled reflectance from a plane-parallel snow surface.

Figure 4 shows an observed pattern of *R* on the left and the pattern calculated by DISORT for the same wavelength and solar zenith angle on the right. The snow pack in DISORT was described as a semi-infinite layer of particles with effective radii of 100 μm (the single-scattering albedo and asymmetry parameter were calculated from Mie theory for 100-micrometer ice spheres, and their phase function was specified as the Henyey-Greenstein phase function with the asymmetry parameter calculated from Mie theory. The snow surface in DISORT, a plane-parallel model, is necessarily perfectly flat.

The differences between the two patterns in Figure 4 are consistent with the effects of surface roughness on the BRDF. Surface roughness reduces the strength of the forward reflectance peak because an observer looking toward the solar azimuth sees the shaded sides of surface roughness elements, and it enhances the backward reflectance because an observer looking away from the solar azimuth sees the parts of surface roughness elements that are tilted toward the sun, which effectively reduces the solar zenith angle on those elements.

The phase function of the real snow grains differs from the Henyey-Greenstein phase function, and this discrepancy may explain some of the differences between the two patterns in Figure 4. Future modeling will use different phase functions to investigate the degree to which these differences are due to surface roughness effects and to single-scattering effects.

5. EFFECT OF CLOUDS OVER SNOW

Satellite observations have shown that the presence of a cloud over snow increases the scene brightness when looking near the solar azimuth at large viewing zenith angles and reduces the brightness at other angles (Welch and Wielicki, 1989; Loeb, 1997; Wilson and Digirolamo, 2004; Kato and Loeb, 2005). This effect was also observed by eye and in our measurements at Dome C when shallow layers of fog, extending from the surface to a height below our observation location, formed some evenings. It may seem counterintuitive that clouds enhance the forward reflectance

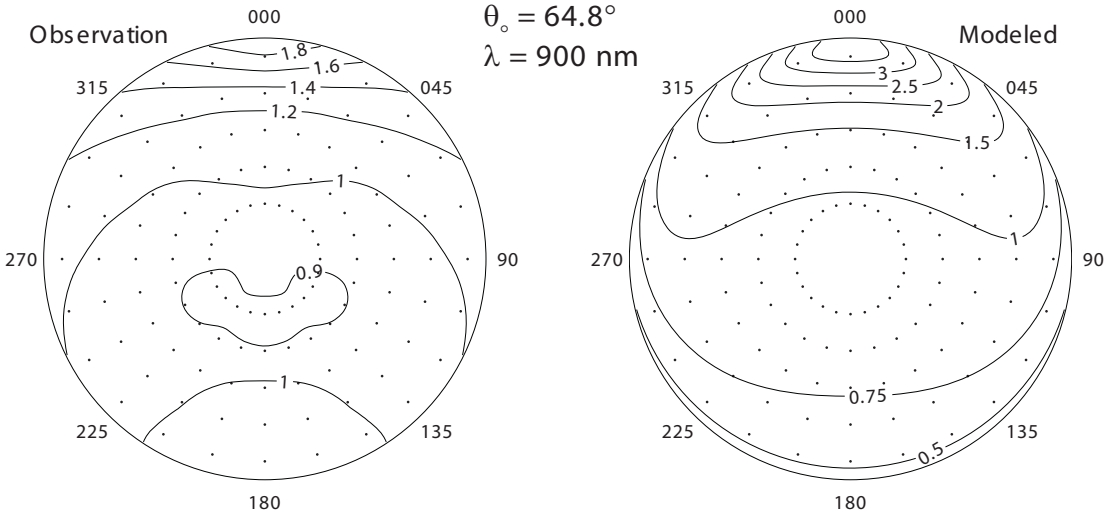

Figure 4. Values of *R* at 900 nm, $\theta_o = 64.8°$, observed for the natural rough surface at Dome C, and modeled for a hypothetical flat surface with DISORT.

peak because the droplets in clouds are significantly smaller than snow grains and are therefore less forward-scattering than the snow grains.

We suspect that this effect is not due to the single-scattering properties of the cloud or snow particles, but to the macroscale roughness difference between clouds and snow surfaces. Because convection is generally limited by the stable stratification of polar atmospheres, the clouds in polar regions are often stratiform. When measured in geometrical units, the spatial variability of the height of the upper surfaces of even these stratiform clouds may be much larger than the spatial variability of the height of the snow surface; however when this variability is measured in units of optical depth, which is what is relevant for radiative transfer, it is much smaller at the tops of polar clouds than at the snow surface since 1 cm of snow has a greater optical depth than most polar clouds.

Figure 5 shows the effect of a thin layer of fog above the snow surface as observed one evening at Dome C. The anisotropic reflectance pattern predicted by the parameterization discussed above for a wavelength of 800 nm and a solar zenith angle of 81.8° is shown on the left, and is representative of what would be observed under these conditions with clear skies. The observation made at this wavelength and solar zenith angle when a fog layer was present between the surface and about 20 m above the surface is shown on the right. The plot at the center shows the relative change of *R* caused by the fog. The fog significantly enhanced the reflectance near the forward peak and reduced the reflectance into other large viewing zenith angles; the fog was so thin that it had little effect at small or moderate viewing zenith angles.

To explore the hypothesis that this effect is caused by differences in surface roughness, DISORT was used, with a specified lower BRDF from the parameterization, to simulate a thin fog layer over the Dome C snow surface for comparison with the observations of the reflectance in this situation. The results are shown in Figure 6, where the plot on the right is the same as that in Figure 5, but the one on the left is the simulated anisotropic reflectance pattern for the Dome-C snow surface covered by a plane-parallel cloud, composed of 5-micrometer spherical water droplets, with an optical depth of 0.025. Clearly the modeled cloud has the right effect, reducing the magnitude of the error by reducing the forward peak and increasing the reflectance at other large viewing zenith angles.

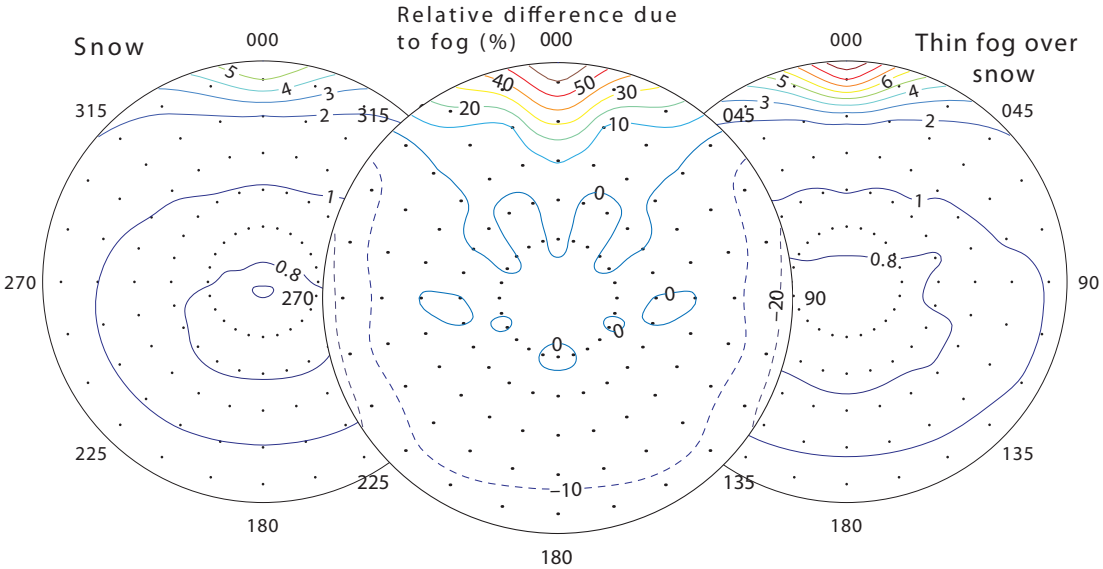

Figure 5. On the left is the anisotropic reflectance factor from the paramaterization based on clear-sky data for 800 nm with a solar zenith angle of 81.8°. On the right is an observation for the same conditions made while a fog layer was present extending from the surface to about 20 m. The plot in the center shows the relative change of *R* due to the presence of the fog.

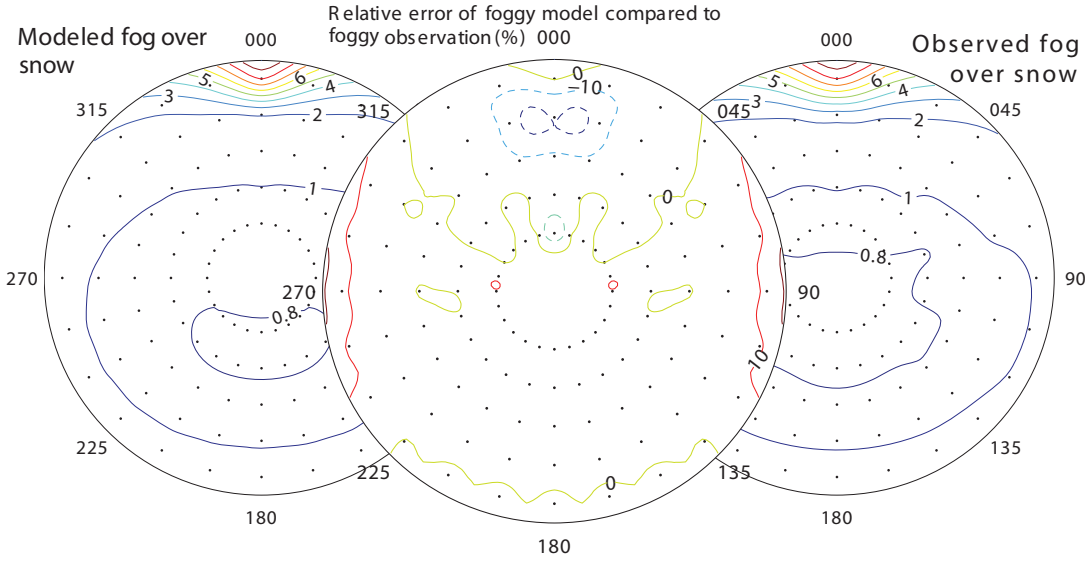

Figure 6. On the left is the anisotropic reflectance factor of a thin fog over a rough snow surface for 800 nm with a solar zenith angle of 81.8° modeled with DISORT. On the right is an observation for the same wavelength and solar zenith angle made while a fog layer was present extending from the surface to about 20 m. The plot in the center is the relative difference between the two.

In a similar simulation in which the model fog was placed above a plane-parallel modeled snow surface, the fog had a much smaller effect, with the opposite sign (enhancing the forward peak).

While further study is needed, it appears that the effect of a cloud over the snow surface is simply to make the surface of the system smoother. This alters the reflectance pattern to make it more similar to the plane parallel case modeled in Section 4, producing a greater forward peak while reducing the reflectance elsewhere.

ACKNOWLEDGMENTS

We thank Michel Fily at the Laboratoire de Glaciologie et Géophysique de l'Environnement for sponsoring our work at Dome C. Von Walden, Bradley Halter, Lance Roth, Michael Town and Elise Hendriks all in some way helped us with this work, and the logistics team at Dome C made the field work much easier. Logistics at Dome C were provided by the French and Italian Antarctic Programs. This work was supported by NSF grant OPP-00-03826.

REFERENCES

Hudson, S.R., S.G. Warren, R.E. Brandt, T.C. Grenfell, and D. Six, 2006: Spectral bidirectional reflectance of Antarctic snow: Measurements and parameterization. *J. Geophys. Res.*, in press.

Kato, S., and N.G. Loeb, 2005: Top-of-atmosphere shortwave broadband observed radiance and estimated irradiance over polar regions from Clouds and the Earth's Radiant Energy System (CERES) instruments on Terra. *J. Geophys. Res.*, **110**, D07202, doi:10.1029/2004JD005308.

Leroux, C., and M. Fily, 1998: Modeling the effect of sastrugi on snow reflectance. *J. Geophys. Res.*, **103**, 25 779—25 788.

Loeb, N.G., 1997: In-flight calibration of NOAA AVHRR visible and near-IR bands over Greenland and Antarctica. *Int. J. Remote Sensing*, **18**, 477—490.

Warren, S.G., R.E. Brandt, and P. O'Rawe Hinton, 1998: Effect of surface roughness on bidirectional reflectance of Antarctic snow. *J. Geophys. Res.*, **103**, 25 789—25 807.

Welch, R.M., and B.A. Wielicki, 1989: Reflected fluxes for broken clouds over a Lambertian surface. *J. Atmos. Sci.*, **46**, 1348—1395.

Wilson, M.J., and L. Di Girolamo, 2004: The utilization of MISR for polar cloud modeling. *Geoscience and Remote Sensing Symposium, 2004. IGARSS' 04 Proceedings*, IEEE International, 4361—4362.